Molecular drug design, synthesis and crystal structure determination of Cu-II-Sn-IV heterobimetallic core: DNA binding and cleavage studies

ARTICLE *in* EUROPEAN JOURNAL OF MEDICINAL CHEMISTRY · MARCH 2012

Impact Factor: 3.45 · DOI: 10.1016/j.ejmech.2012.01.005 · Source: PubMed

5 AUTHORS, INCLUDING:

Farukh Arjmand
Aligarh Muslim University
111 PUBLICATIONS **1,359** CITATIONS
SEE PROFILE

Mohd Afzal
North Eastern Regional Institute of Science …
25 PUBLICATIONS **267** CITATIONS
SEE PROFILE

Taibi Ben Hadda
Université Mohammed Premier
338 PUBLICATIONS **1,437** CITATIONS
SEE PROFILE

European Journal of Medicinal Chemistry 49 (2012) 141–150

Contents lists available at SciVerse ScienceDirect

European Journal of Medicinal Chemistry

journal homepage: http://www.elsevier.com/locate/ejmech

Original article

Molecular drug design, synthesis and crystal structure determination of Cu^{II}–Sn^{IV} heterobimetallic core: DNA binding and cleavage studies

Farukh Arjmand [a,*], Shazia Parveen [a], Mohd. Afzal [a], Loic Toupet [b], Taibi Ben Hadda [c]

[a] Department of Chemistry, Aligarh Muslim University, Aligarh 202002, India
[b] Institut de Physique de Rennes, UMR 625, Université de Rennes 1, Campus de Beaulieu Bat. 11 A, 263 av. Général Leclerc, 35042 Rennes Cedex, France
[c] Laboratoire Chimie des Matériaux, FSO, Université Mohammed I, Oujda 60000, Morocco

ARTICLE INFO

Article history:
Received 12 August 2011
Received in revised form
5 January 2012
Accepted 5 January 2012
Available online 15 January 2012

Keywords:
Cu^{II}–Sn^{IV} phen complex
CT DNA binding
pBR322 DNA cleavage
T4 DNA ligase assay
Topo I inhibition activity
Molecular docking

ABSTRACT

A novel heterobimetallic Cu^{II}–Sn^{IV} complex **1** bearing bioactive 1,10-phenanthroline pharmacophore ligand scaffold was synthesized and characterized by elemental analysis, IR, UV–vis spectroscopy, Mass (ESI and FAB) and X–ray crystallography. The *in vitro* DNA binding studies of complex **1** with CT DNA was carried out by various biophysical and molecular docking techniques which revealed that complex **1** binds to DNA through intercalation in the minor groove having AT-rich sequences. Complex **1** exhibits high chemical nuclease activity cleaving supercoiled pBR322 DNA via hydrolytic pathway which was further evidenced by T4 DNA ligase assay. The complex **1** shows high inhibitory activity against Topo I at a very low concentration (15 μM), suggesting that complex **1** is an efficient catalytic inhibitor of human Topo I and further validated by molecular docking studies.

1. Introduction

Metal complexes that can bind to DNA are gaining considerable attention owing to their diverse applications in the field of bio-inorganic chemistry viz. diagnostic agents for medical applications, development of cleavage agents for probing nucleic acid structure [1,2] and identifiers of transcription start sites [3]. DNA is an important target of antitumor drugs and interactions of DNA with transition metal complexes are important for the design of efficacious drug entities which exhibit different properties than the mainstream protocol drugs viz. cisplatin, etc. which are currently in use [4].

Copper have been used since antiquity in metal-based therapies. Copper is a bioessential element which plays a key role in biological processes, and its complexes are preferred molecules for cancer inhibition by chemotherapy [5]. Among the copper complexes explored so far, considerable attention has been focused on 1,10-phenanthroline Cu^{II} complexes due to their high nucleolytic efficiency and numerous biological activities such as antitumor, antimicrobial, etc. Several copper complexes have been described as DNA cleaving agents and the best studied example is Sigman's $[Cu(phen)_2]^{2+}$ complex [6]. This complex is reduced in situ to $[Cu(phen)_2]^{+}$ and subsequently binds to minor groove of DNA, combines with molecular oxygen, to generate a non-diffusible oxidant and finally induces strand scission by oxidation of the ribose backbone.

Literature supports that Cu^{II} ions specifically bind to the N-7 guanine residue of DNA and cause strand breakage [7]. The kinetic analysis of copper DNA interaction and its site-specific binding with DNA have been well–documented [8]. On the contrary, Sn^{IV} complexes prefer to bind to the phosphate backbone of the DNA helix (Sn^{IV} ions have a hard Lewis acid nature, neutralize the negative charge of phosphate sugar, and bring conformational changes in DNA) [9]. Previous studies of Cu^{II} and Cu^{II}–Sn^{IV} complexes have shown interesting results against various cancerous cell lines (HeLa cells, T47D, HT29) [10]. It has been demonstrated that these complexes induce apoptosis via mitochondrial pathway. Thus, heterobimetallic complexes containing Cu^{II} and Sn^{IV} ions enhance the chemotherapeutic action many-fold as they provide a dual mode of binding at the molecular target site and also exhibit novelty due to preferential selectivity inside the

Abbreviations: UV–vis, UV–visible; CT DNA, Calf thymus DNA; Tris, tris(hydroxymethyl)aminomethane; EB, ethidium bromide; Phen, 1,10-phenanthroline; Topo I, topoisomerase I.

* Corresponding author. Tel.: +91 571 2703893.
E-mail address: farukh_arjmand@yahoo.co.in (F. Arjmand).

0223-5234/$ – see front matter © 2012 Elsevier Masson SAS. All rights reserved.
doi:10.1016/j.ejmech.2012.01.005

cells [11]. Furthermore, some additional favorable non-covalent interactions such as hydrogen bonding, van der Waals forces within the groove of DNA can enhance DNA binding multi-fold and enforce specificity [12]. In the present work, we have designed a new ionic crystalline molecular entity **1** possessing Cu^{II}–Sn^{IV} heterodinuclear unit; such Cu^{II}–Sn^{IV} ionic motifs are scarce in literature, however, some ionic triphenyltin(IV)chloride carboxylate complexes exhibiting exceptional cytotoxicity have been reported earlier [13]. The molecule exhibits novelty, fulfilling all the pre-requirements for efficient chemotherapeutic drug design which include (i) good DNA binding propensity, (ii) specific tagging to drug target at molecular level, (iii) preferential selectivity to DNA base sites/minor groove binding, efficient DNA cleavage and potent Topo I activity, (iv) multifaceted binding modes, (v) unsaturated coordination geometry at the cation and anion metal centers. The computer-aided molecular docking study carried out in this work affords valuable information of drug binding mode (intercalative mode of binding, in addition to favorable hydrogen bonding interactions) in the active site of DNA–Topo I which lead to the rational design of new classes of anticancer drugs targeting Topo I. Literature reveals that minor groove analogs such as camptothecin derivatives, approved as anticancer drugs and selective DNA–Topo I inhibitors exhibited certain drawbacks such as chemically unstable structure and rapid efflux from the cell by the membrane pumps [14]. Thus, adapting a strategy based on metal and an intercalating scaffold with ionic recognition domain can lay design paradigm for new DNA–Topo I inhibitors.

2. Chemistry

In order to elucidate the molecular recognition toward the minor groove of DNA and inhibit DNA processing enzymes, new drug candidate was designed and synthesized. The synthesis of novel heterobimetallic complex **1** was achieved by mixing stoichiometric amounts of Cu^{II} chloride dihydrate with 1,10-phenanthroline monohydrate followed by drop wise addition of dimethyltin dichloride (Scheme 1). The formulation of the complex **1** was confirmed by determination of the X-ray crystal structure. The resulting complex **1** is stable toward air and moisture and readily soluble in DMSO. Molar conductance value of complex in DMSO (1×10^{-3} M) at 25 °C suggests its 1:1 electrolyte nature ($74\ \Omega^{-1}\ cm^2\ mol^{-1}$).

3. Results and discussion

3.1. Electronic spectra

The complex **1** exhibited a broad d–d band at 726 nm and a low-energy shoulder band at 891 nm suggesting the Cu^{II} ion in a five-coordinate environment and strong charge transfer (CT) band near 271 nm followed by a shoulder band at 295 nm attributed to the π–π^* transition of the coordinated phenanthroline ligand (Supplementary material Fig. S1) [8,15]. The Sn^{IV} anion moiety did not exhibit any d–d band transitions.

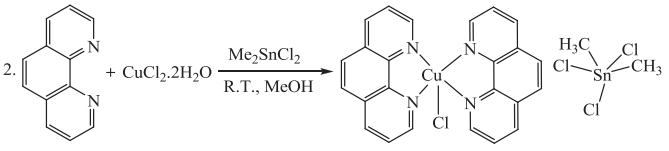

Scheme 1. Synthetic route for the heterobimetallic complex **1**.

3.2. Mass spectral analysis

The nature of heterobimetallic complex **1** in solid and solution state were studied with FAB and ESI–MS, respectively (Fig. S2a and b). The FAB mass spectrum of complex **1** in solid state showed the molecular ion peak m/z at 712 which was assigned to $[C_{26}H_{22}Cl_4CuN_4Sn - 2H]^+$. The appearance of other peaks at m/z 677, 606 and 570 (50%) were ascribed to the species $[C_{26}H_{22}Cl_4CuN_4Sn - Cl + 2H]^+$ $[C_{26}H_{22}Cl_4CuN_4Sn - Cl_3 + 2H]^+$ and $[C_{26}H_{22}Cl_4CuN_4Sn - Cl_4 + 2H]^+$, respectively. However, ESI–MS spectra of the complex **1** in DMSO solution displayed molecular ion fragment peaks at m/z 458.8 and 254.3 corresponding to the complex cation and anion, respectively, which confirms the ionization of complex **1** in solution state and are well separated from each other leads to further fragmentation separately. The fragmentation peaks for complex cation observed at m/z 421.9 and 63.2 (50%) were ascribed to the species $[Cu(phen)_2C1 - Cl + H^+]^+$ and $[Cu(phen)_2C1\text{-}(phen)_2 + Cl + H^+]^+$, respectively. While in case of complex anion, fragmentation peaks after the successive expulsion of three chlorine atoms were obtained at m/z 218.4, 184.1 and 148.6. Another peak at m/z 118.7 was obtained by the removal of two $-CH_3$ groups and finally the Sn^{IV} metal ion was ionized. These mass spectral analysis (FAB and ESI) results indicate that complex **1** existed as a whole entity in solid state but undergoes self ionization in solution state.

3.3. Description of crystal structure

The single crystal X-ray analysis reveals that the title complex **1** crystallizes as monoclinic crystal system with space group $P2_1/c$. An ORTEP view of the complex together with atom-numbering scheme is illustrated in Fig. 1, while relevant bond lengths and bond angles are listed in Table 1. The crystal structure is quite interesting and displays the formation of a heterodinuclear unit having two different geometries with no evidence for even semi-coordination existing between them. However, both are held together by means of electrostatic forces and van der Waals interactions and separated by a distance of 6.04 Å. The molecular structure of the complex is composed of discrete $[Cu(phen)_2C1]^+$ cation and $[Me_2SnCl_3]^-$ anion in order to balance the charge and behaves as neutral molecule. The complex cation exhibits a five-coordinated $Cu^{II}N_4C1$ chromophore as slightly distorted square pyramid $(4+1)$ with the structural index parameter $\tau = 0.63$ [$\tau = (\beta - \alpha)/60$], where α and β are the two largest metal ligand bond angles in the complex, $\tau = 0$ and 1 for ideal square pyramidal and trigonal bipyramidal geometries, respectively. The plane of the phenanthroline ligands is inclined to each other with a dihedral angle of 46.9° showing these two rings are not in a good planarity. The $Cu^{II}N_4$ core, from two bidentate phen ligands, forming two five-membered chelated rings with intraligand N–Cu–N angles of 80.77(15) and 81.40(16)°, respectively, while the interligand N–Cu–N angles ranges between 112.39(15)–173.39(16)°, whereas apical position is occupied by the Cl atom, Cl(1). The Cu1–Nphen bond lengths fall within a narrow range of 2.001 (4)–2.143 (4) Å with an average value of 2.072 Å, which are significantly shorter than the Cu1–C1(1) bond length 2.3106 (13) Å (Table 1), consistent with the larger size of the chlorine atom, indicating that phenanthroline is more strongly coordinated to metal center than chlorine atom [16].

In the case of complex anion, the Sn^{IV} metal ion is five-coordinated in a trigonal bipyramidal geometry with the two methyl groups and one chlorine atom are placed in equatorial position while axial position is occupied by two chlorine atom. The bond length between Sn(1)–Cl(2), Sn(1)–Cl(3) and Sn(1)–Cl(4) are 2.368(12), 2.545(3) and 2.597(4), respectively, which indicates that

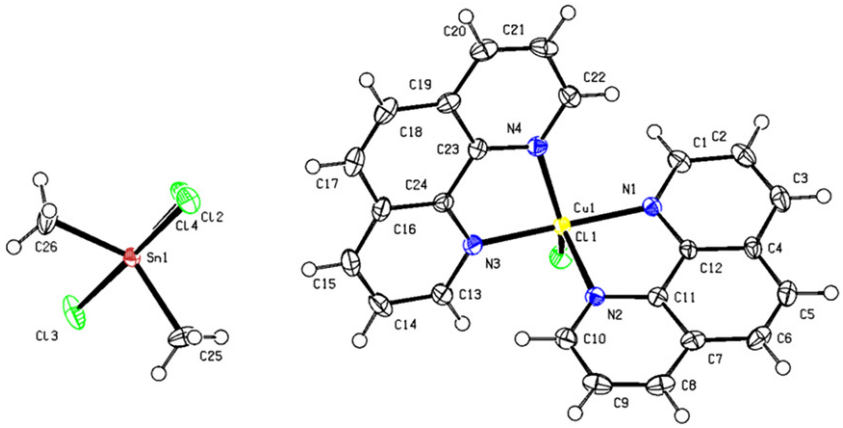

Fig. 1. ORTEP view of complex **1** with ellipsoids drawn at 50% probability levels.

equatorial position was significantly longer (by ~0.22 Å) than axial chlorine atom which is in agreement with other Sn–Cl bonds in zwitterionic complexes [13,17] and the carbon–tin–carbon angle is opened to 136.5(3)° (Table 1) [18,19]. Moreover, in the arrangement of the unit cell, there exist orderly aromatic ring stacking interactions between phenanthroline ligands among the molecules of the complex. Six phenanthroline atoms (C1, C2, C3, C4, C12, N1) form weak π–π stacking with other phenanthroline atoms (C7′, C8′, C9′, C10′, C11′, N2′) in a neighboring molecule with centroid distance of 3.544 Å [20].

3.4. DNA binding studies

3.4.1. UV–vis absorption titrations

Electronic absorption spectroscopy is one of the most useful techniques for DNA binding studies of metal complexes. The interaction of the heterobimetallic complex with CT DNA was carried out by employing electronic absorption spectroscopy. The complex **1** exhibited intense absorption bands at 271 nm attributed to π–π* transitions and a shoulder band at 295 nm as shown in Fig. 2. A fixed concentration of the complex was titrated with increasing amounts of CT DNA. The complex exhibited hypochromism (52% hypochromicity), i.e. a decrease in the absorption intensity with no shift in the wavelength. The extent of red shift and hypochromism are commonly found to correlate with the intercalative binding strength [21,22]. Hypochromism and a red shift (bathochromism) of the absorption band implicates in general, intercalative mode of binding due to strong stacking interaction between the planar aromatic chromophore (1,10-phenanthroline) and the base pairs of the DNA [2,23], while hyperchromism is a spectral feature depicting non-covalent interactions, particularly electrostatic, groove binding etc resulting from the damage of DNA double helix structure. Earlier studies on bis-phen Cu complex have shown that the complex binds to DNA either by partial intercalation or binding of one phenanthroline ligand to the minor groove while the other phenanthroline could possibly make favorable contacts within the groove [24,25]. The results derived from the UV–vis titration experiments suggest that the complex **1** bind to CT DNA through intercalation into the minor groove.

Table 1
Selected bond lengths (Å) and angels (°) for complex **1**.

Bond lengths	(Å)
Cu(1)–Cl(1)	2.3106(13)
Cu(1)–N(3)	2.001(3)
Cu(1)–N(1)	2.001(3)
Cu(1)–N(4)	2.078(3)
Cu(1)– N(2)	2.143(4)
Sn(1)–Cl(2)	2.3689(12)
Sn(1)–Cl(3)	2.5457(3)
Sn(1)–Cl(4)	2.5971(4)
Sn(1)–C(25)	2.110(5)
Sn(1)–C(26)	2.111(5)
Bond angles	**(°)**
N(1)–Cu(1)–N(3)	173.39(16)
N(3)–Cu(1)-N(4)	81.40(16)
N(1)–Cu(1)–N(4)	95.57(16)
N(3)–Cu(1)–N(2)	94.90(16)
N(1)–Cu(1)–N(2)	80.77(15)
N(4)–Cu(1)–N(2)	112.39(15)
N(3)–Cu(1)–Cl(1)	94.32(12)
N(1)–Cu(1)–Cl(1)	91.95(11)
N(4)–Cu(1)–Cl(1)	135.50(12)
N(2)–Cu(1)–Cl(1)	112.11(11)
C(25)–Sn(1)–C(26)	136.50(3)
C(25)–Sn(1)–Cl(2)	109.74(18)
C(26)–Sn(1)–Cl(2)	113.7(2)
C(25)–Sn(1)–Cl(3)	91.36(18)
C(26)–Sn(1)–Cl(3)	89.28(17)
Cl(2)–Sn(1)–Cl(3)	91.08(5)
C(25)–Sn(1)–Cl(4)	89.22(18)
C(26)–Sn(1)–Cl(4)	89.67(17)
Cl(2)–Sn(1)–Cl(4)	89.57(4)
Cl(3)–Sn(1)–Cl(4)	178.92(4)

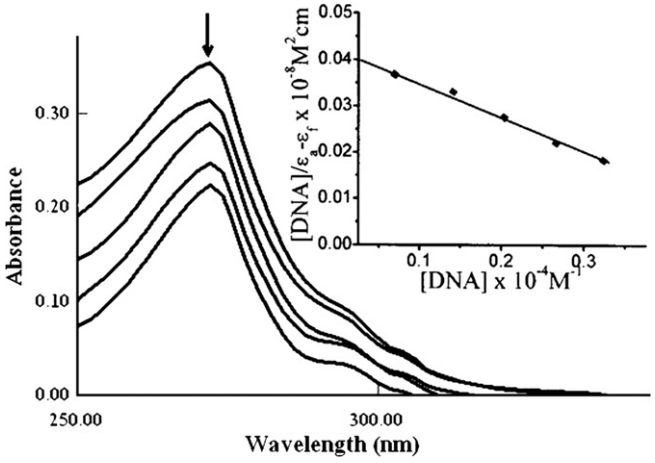

Fig. 2. Absorption spectral traces of complex **1** in 5 mM Tris–HCl/50 mM NaCl buffer at pH 7.2 upon addition of CT DNA. Inset: Plots of $[DNA]/\varepsilon_a - \varepsilon_f$ (m^2 cm) vs [DNA] for the titration of CT DNA with complexes ■, experimental data points; full lines, linear fitting of the data. [Complex] 10^{-5} M, [DNA] 0–1.66×10^{-5} M.

To quantify the extent of binding of complex **1** to CT DNA, the intrinsic binding constant, K_b was calculated by monitoring the changes in the absorbance at the corresponding λ_{max} with increasing concentrations of CT DNA and is given by the ratio of slope to the intercept in plots from the Wolfe–Shimer equation which was found to be 2.07×10^5 M^{-1}. Interestingly, the intrinsic binding K_b value is much higher in magnitude in comparison to our previous Cu^{II}–Sn^{IV} heterobimetallic complex (K_b value 3.0×10^4 M^{-1}) [11] which demonstrate the remarkably higher binding strength of complex **1** to DNA due to intercalative mode of binding. This further supports the contention that heterobimetallic Cu^{II}–Sn^{IV} chemical entity **1** is designed to serve as an excellent drug motif.

3.4.2. Interaction with 5′-AMP and 5′-TMP (validation by ^1H and ^{31}P NMR)

To validate our hypothesis of complex **1** showing preferential binding toward the AT-rich sequence of DNA, interaction studies of **1** with mononucleotides, viz; 5′-AMP and 5′-TMP were carried out by ^1H and ^{31}P NMR techniques at physiological pH 7.2 (SI Fig. S3 and S4 (a and b)). The ^1H NMR of free 5′-AMP in D_2O exhibits H(8) and H(2) aromatic protons (adjacent to N(7) and N(1) atom of adenine) resonance at 8.36 and 8.07 ppm, respectively. For paramagnetic complexes, the chemical shift of proton adjacent to the metal center was significantly perturbed resulting in line broadening. On interaction of complex **1** with 5′-AMP, the H(2) signal undergoes a substantial shift from 8.36 to 8.13 ppm while H(8) signal was broadened and undergoes a significant downfield shift from 8.07 to 7.69 ppm with a slight decrease in the peak intensity (Fig. S3a). This downfield shift results due to the deshielding of H8 proton by coordinate bond formation of Cu^{II} metal ions of complex **1** preferably via N(7) atom rather than N(1) of 5′-AMP [26]. On the other hand, on addition of complex **1** to 5′-TMP, the signal of N3–H of free 5′-TMP at 7.70 ppm remains unaffected attributing to non-participation of thymine on binding with Cu^{II} metal ion of complex **1** through coordination mode (Fig. S3b). However, the ribose proton H1′–H5′signals were shifted upfield ~0.08 ppm, which indicate the preference for ribose sugar due to the presence of Sn^{IV} hard Lewis acid center [11].

^{31}P NMR throws further insight to the molecular mechanism of binding and as stated by Marzilli, the phosphate group interaction dominates the formation constant of metal–nucleotide complexes and the base portion plays a secondary role [27]. The ^{31}P NMR signal appeared in free 5′-AMP and 5′-TMP at 0.88 and 3.18 ppm, respectively, which was shifted downfield (1.34 ppm with 5′-AMP and 4.84 ppm with 5′-TMP) in presence of complex **1**, shown in SI, Fig. S4a and b, clearly indicating that the presence of outer-sphere coordination of phosphate oxygen by strong Sn–OPO_3^{-2} bonding of the Sn^{IV} metal ion with phosphate group [28]. Thus, present results validate the dual binding modes of complex **1** with the DNA double helix viz, N7 of 5′-AMP being the preferred binding site of Cu^{II} ion via coordinative interactions and simultaneously, the Sn^{IV} metal ion interacts with vicinal oxygen of phosphate group of the nucleotides by an electrostatic binding mode. These results have also been corroborated further by molecular docking techniques.

3.4.3. Emission spectral studies

In the emission spectra, complex **1** displayed a luminescence maximum at 513 nm at room temperature in the absence of DNA when excited at 260 nm. The emission spectrum of complex **1** in presence of varying amounts of DNA is shown in Fig. 3. With the addition of DNA, the fluorescence intensity gradually increased with no apparent change in the shape and position of the emission bands. This implies that the complex strongly interact with CT DNA probably due to the inaccessibility of the solvent water molecules to reach the hydrophobic environment inside the DNA helix, and the mobility of the complex is restricted at the binding site ultimately leading to decrease in vibrational mode of relaxation. However, this enhancement is much less as compared to classical intercalators [29]. When a complex binds to DNA helix through intercalation, the DNA being a hydrophobic macromolecule can prevent quenching and increase the fluorescence of the complex when bound to it. Furthermore, the binding of complex to the DNA helix could decrease the collisional frequency of solvent molecules, with the complex, leading to the emission enhancement of the complex [30]. The binding constant value, K determined from the Scatchard equation is calculated to be 1.7×10^5 M^{-1}. The calculated binding constants are slightly different from those obtained by absorption titrations due to the different spectroscopic and different calculation methods.

In order to further investigate the interaction mode of complex **1** with DNA, a competitive binding experiment using EB as a probe was carried out. EB does not show any appreciable emission in the buffer solution due to fluorescence quenching of the free EB by solvent molecules, while in the presence of CT DNA, the fluorescence intensity of EB is highly enhanced due to its strong intercalation between the adjacent DNA base pairs [31]. The enhanced fluorescence can be quenched upon the addition of the second molecule which could replace the bound EB or break the secondary

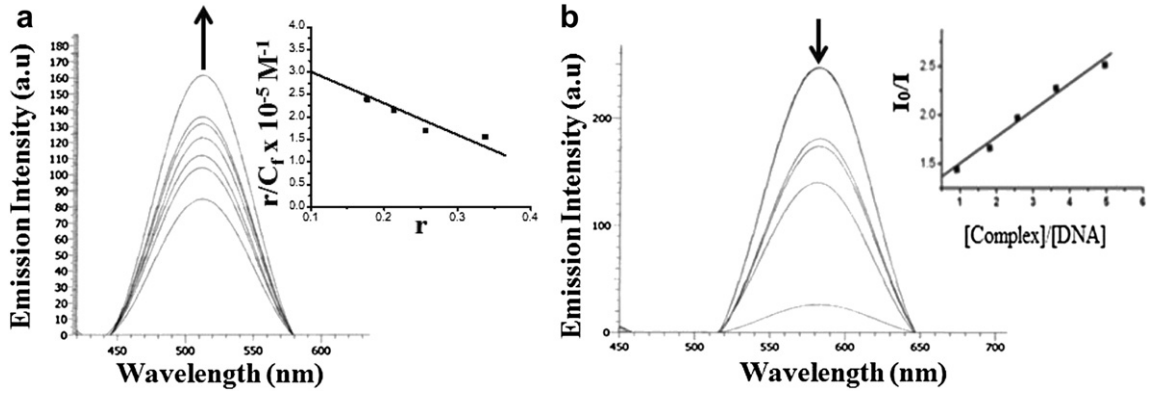

Fig. 3. Emission spectra of (a) complex **1** in the presence of DNA in 5 mM Tris–HCl/50 mM NaCl buffer. Inset: Plot of r/C_f vs r (b) EB bound to DNA in the presence of complex **1** in Tris–HCl buffer at pH 7.2. Arrows indicate the intensity changes upon increasing concentration of the complexes. Inset: fluorescence quenching curve of DNA bound EB with complexes ■, experimental data points; full lines, linear fitting of the data, (Excitation wavelength, 260 nm).

structure of the DNA. The emission spectra of EB–DNA in the absence and presence of complex is presented in Fig. 3, the emission band at 580 nm of EB–DNA system decreased in intensity with increasing concentration of the complex suggesting that the complex binds through intercalation replacing the intercalated EB molecule which is in good agreement with the absorption spectroscopy. The extent of quenching of the emission intensity gives a measure of the binding propensity of the complex **1** to CT DNA. According to the classical Stern–Volmer equation [32]:

$$I_0/I = 1 + K_{SV}\cdot r$$

where I_0 and I represent the fluorescence intensities in the absence and presence of the complex **1**, respectively; r is the concentration ratio of the complex to DNA and K_{SV} used to evaluate the quenching efficiency is obtained as the slope of I_0/I vs r. The K_{SV} value for the complex **1** was found to be 1.25, indicating the strong affinity of the complex **1** to CT DNA.

Steady-state emission quenching experiments using $[Fe(CN)_6]^{4-}$ as a quencher were also performed to observe the binding mode of the complexes to DNA. $[Fe(CN)_6]^{4-}$ is a dynamic fluorescence quencher and provides a sensitive tool to examine the nature of the interaction of the probe with DNA [33]. $[Fe(CN)_6]^{4-}$ poorly quench fluorescence of complexes which are strongly bound to the DNA whereas the complexes which are free in solution are quenched efficiently due to ion pairing [34]. The quenching efficiency is evaluated by the Stern–Volmer equation. The emission intensity of the complex **1** was greatly affected by the addition of anionic quencher. The decrease in emission intensity of the complex was due to the repulsion of highly negative charged $[Fe(CN)_6]^{4-}$ from the DNA polyanion backbone, which hinders access of $[Fe(CN)_6]^{4-}$ to the DNA-bound complexes [35]. The plot of free complex **1** gave a K_{sv} value of 1.13×10^5 M^{-1} (Fig. S5). In the presence of DNA the quenching curve was depressed reflecting the protection of complex by the DNA helix and the K_{sv} value of **1** decreased to 9.7×10^4 M^{-1}.

3.4.4. Viscosity measurements

Hydrodynamic properties and especially viscosity can give better indications on the binding mode of a small molecule to DNA. While intercalation results in a substantial change of the double helix, the other types of interactions produce only subtle changes in the structure and the DNA remains especially in the unperturbed B-DNA form. In particular, the former type of the interaction causes lengthening and stiffening of the helix which results in an increase of the viscosity of DNA. It is found that the complex behaved as a typical intercalator: addition of the complex produced sequential increase in the specific viscosity due to the expected increase in the duplex contour length [36]. As shown in Fig. 4, the heterobimetallic complex **1** exhibited an increase in the viscosity of CT DNA suggesting the intercalative mode of binding.

3.5. Chemical nuclease activity

In order to ascertain the ability of the complex **1** to serve as a metallonuclease, the DNA cleavage was performed with pBR322 DNA as a substrate using different complex concentrations. The activity of complex **1** was assessed by the conversion of DNA from Form I to Form II and Form III. When circular plasmid DNA is conducted by electrophoresis, the fastest migration will be observed for the supercoiled form (Form I). If one strand is cleaved, the supercoils will relax to give a slower-moving nicked circular form (Form II). If both strands are cleaved, a linear form (Form III) will be generated that migrates in between. Firstly, concentration-dependent DNA cleavage activity of complex **1** was performed

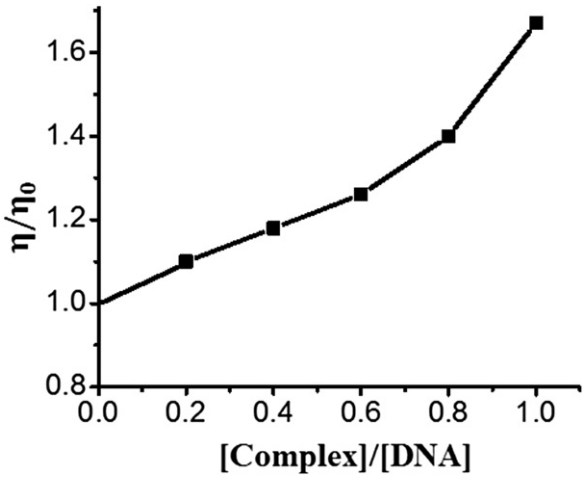

Fig. 4. Effect of increasing amount of complex **1** on the relative viscosities (η/η_o) of CT DNA in Tris–HCl buffer (pH 7.2).

where pBR322 DNA (300 ng) was incubated with increasing concentration of complex in a medium of 5 mM Tris–HCl/50 mM NaCl buffer solution (pH 7.2) for 45 min without addition of a reductant. As shown in Fig. 5, it was observed that complex **1** exhibits potent nuclease activity at low concentration (5 μM), followed by the complete conversion of supercoiled DNA to its open circular form (Lane 2). On increasing complex concentrations (10–20 μM), the cleavage is found to be much more efficient, the linear form were manifested in the gel (Lanes 3–5). At the same time, when the concentration of complex **1** reached to 25 μM, only linear form III was observed in the gel (Lane 6). The appearance of linearized form (Form III) in the cleavage assay indicates double strand scission of the DNA helix. So, it is clear that cleavage of pBR322 DNA is highly dependent on the number of metal ions as well as the presence of an aromatic ring.

3.5.1. In presence of activators

The nuclease efficiency of the metal complexes is known to depend on the activators used for initiating the DNA cleavage. Therefore, DNA cleavage activity of complex **1** in presence of H_2O_2, ascorbate, 3-mercaptopropionic acid and glutathione was evaluated (Fig. 5). The cleavage activity of complex **1** was significantly

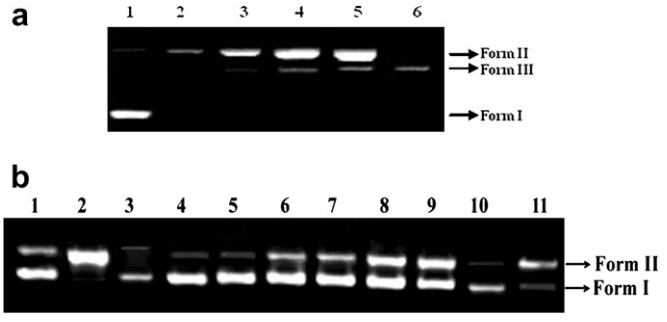

Fig. 5. Agarose gel electrophoresis cleavage patterns showing cleavage of pBR322 supercoiled DNA (300 ng) by complex **1** at 310 K after 45 min of incubation (a) at different concentration; Lane 1: DNA control; Lane 2: 5 μM of **1** + DNA; Lane 3: 10 μM of **1** + DNA; Lane 4: 15 μM of **1** + DNA; Lane 5: 20 μM of **1** + DNA; Lane 6: 25 μM of **1** + DNA. (b) In presence of different activating agents; Lane 1: DNA control; Lane 2: 25 μM of **1** + H_2O_2 (0.4 M)+DNA; Lane 3: 25 μM of **1** + MPA (0.4 M) + DNA; Lane 4: 25 μM of **1** + GSH (0.4 M) + DNA; Lane 5: 25 μM of **1** + ASc (0.4 M) + DNA; Lane 6: 25 μM of **1** + DMSO (0.4 M) + DNA; Lane 7: 25 μM of **1** + EtOH (0.4 M) + DNA; Lane 8: 25 μM of **1** + sodium azide (0.4 M) + DNA; Lane 9: 25 μM of **1** + SOD (15 units) + DNA; Lane 10: 25 μM of **1** + DNA + DAPI (8 μM); Lane 11: 25 μM of **1** + DNA + methyl green (2.5 μL of a 0.01 mg/ml solution).

enhanced by these activators and follows the order H_2O_2 > MPA > Asc ≈ GSH.

3.5.2. DNA cleavage in presence of recognition elements (groove binding agents)

DNA recognition elements (groove binding) minor groove binding agent, DAPI and major groove binding agent, methyl green were used to probe the potential interacting site of complex **1** with supercoiled plasmid pBR322 DNA. As shown in Fig. 5, DNA cleavage is inhibited in the presence of minor groove binder (Lane 10), However, no apparent inhibition of DNA damage was observed in presence of major groove binder (Lane 11), suggesting that minor grooves are the preferred interacting sites of complex **1** which is in accordance with the conclusion drawn from DNA binding and molecular docking studies.

3.5.3. DNA cleavage in presence of reactive oxygen species

In order to investigate the role of active radicals in the DNA cleavage mediated by complex **1**, reactions were carried out in the presence of hydroxyl radical scavengers (DMSO and EtOH), singlet oxygen quencher (NaN_3) and superoxide oxygen scavenger (SOD), under our experimental conditions as shown in Fig. 5. The experimental results showed that the DNA breakdown mediated by complex **1** was significantly inhibited in the presence of DMSO (Lane 6) and EtOH (Lane 7), indicating that the freely diffusible hydroxyl radical is one of the reactive species involved in the DNA strand scission. Thus, hydrolytic cleavage of the sugar phosphate backbone mediated by hydroxyl radicals could be rationalized. On the other hand, addition of NaN_3 and SOD, show no significant quenching of the cleavage revealing that singlet oxygen and superoxide anion is hardly involved in cleavage process (Lanes 8 and 9). These results suggest that in the DNA strand scission reaction caused by complex **1**, probably through a hydrolytic mechanism involving diffusible hydroxyl radical species.

Since the present complex is able to cleave DNA in the absence of any reducing agent, which reveals that DNA might be cleaved by a discernible hydrolytic path. Hydrolytic pathways usually depend on the Lewis acidity of the central metal ion, which serves to activate the phosphodiester bonds toward nucleophilic attack via charge neutralization and thereby leading to direct hydrolysis of the diester bonds [37]. However, it has been reported previously that a phosphodiester bond can be also hydrolytically cleaved by complexes with N-containing ligands [38,39] and this eventuality cannot be ruled out. Furthermore, direct evidence of DNA hydrolysis was that the linear DNA fragments (Form III) cleaved by the complex can be religated by T4 DNA ligase.

3.5.4. T4 DNA ligation experiment

In order to further explore the mechanism of DNA cleavage exhibited by complex **1**, religation assays were carried out in which supercoiled pBR322 DNA was treated with T4 DNA ligase enzyme and subjected to gel electrophoresis. It is well known that in DNA hydrolytic cleavage 3′-OH and 5′-OPO_3 (5′-OH and 3′-phosphate) fragments must be exclusively afford and that these fragments can be enzymatically ligated [39]. In some cases, the hydrolytic products either did not end at the required 5′-phosphate and 3′-OH (ribose) termini or the complex sometimes bound to the termini of cleaved DNA. These reasons would result in the religation being incomplete or even failing completely [40]. The complex **1** yielded linearized DNA which was religated by using T4 DNA ligase enzyme (Fig. 6a). In our case, DNA religation was complete and after ligation there was complete repair which was quantitatively ascertained by comparison of complex treated DNA and with the control DNA alone in SC form. Hence, it was plausible to interpret that the process of DNA cleavage by complex **1** occurs via a hydrolytic pathway. Complex **1** could therefore, be useful not only in drug design but also in elucidating the precise role of metal ions in enzyme catalysis.

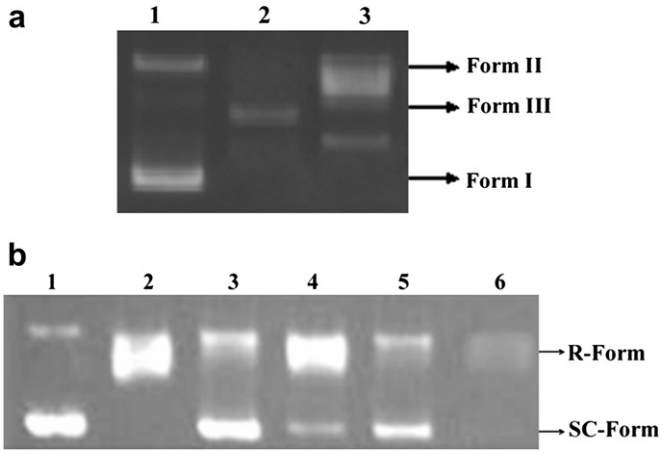

Fig. 6. Agarose gel electrophoresis pattern (a) For the ligation pBR322 plasmid DNA linearized by copper complex **1**: Lane 1, DNA control; Lane 2, pBR322 plasmid DNA cleaved by complex **1**; Lane 3, ligation of linearized pBR322 plasmid DNA by T4 DNA ligase. (b) Showing effect of different concentration of complex **1** on the activity of DNA–Topo I; Lane 1, DNA control; lane 2, Topo I + DNA; Lane 3, 7.5 μM of complex + DNA + Topo I; Lane 4: 10 μM of complex + DNA + Topo I; Lane 5: 12.5 μM of complex + DNA + Topo I; Lane 6: 15 μM of complex 1 + DNA + Topo I.

3.6. Topoisomerase-I inhibition

A standard plasmid DNA cleavage assay was used to investigate the effect of complex **1** on the activity of human Topo I by agarose gel electrophoresis. This assay provides a direct means of determining whether the drug affects the unwinding of supercoiled DNA. When catalytic activity of Topo I was assayed, complex **1** inhibited this process in a concentration-dependent manner [41]. As shown in Fig. 6b, supercoiled DNA was fully relaxed by the enzyme in the absence of complex **1** (Lane 2, Topo I). However, upon increasing the concentration of complex **1** (7.5–15 μM), the levels of relaxed form were inhibited (Lanes 3–6). The DNA relaxation effect caused by Topo I were totally inhibited by complex **1** at 15 μM (IC_{50} ~15 μM), comparing with some classical Topo I inhibitors (Table 2) [42–46]. Because the gel mobility of plasmid DNA was slightly retarded at higher concentrations (e.g., 15 μM) of the complex **1** with the enzyme, it is believed that the DNA-bound complex **1** expels the Topo I from approaching plasmid DNA and in turn leads to a lower level of DNA relaxation. These observations suggest that complex **1** inhibit Topo I catalytic activity due to i) its strong DNA binding affinity ii) concurrent intercalation of the drug into DNA into a topoisomerase binding site may suppress the

Table 2
IC_{50} (μM) values of the complex **1** on Topo I activities, some of the classical Topo I inhibitors.

Complexes	IC_{50} (μM)	Refs.
Etoposide	>1000	[42]
Camptothecin	17	[43]
Doxorubicin	>100	[43]
Novobiocin	>100	[43]
Topostatin	17	[43]
Hoechst 33258	30	[44]
Δ-$[Ru(bpy)_2(uip)]^{2+}$	~40	[45]
Λ-$[Ru(bpy)_2(uip)]^{2+}$	~40	[45]
$[Ru(bpy)_2(appo)]^{2+}$	~25	[46]
Complex **1**	15	This work

association of topoisomerase with DNA, thus influencing the topoisomerase activity [47]. DNA intercalators that inhibit topoisomerase activity or form stabilized ternary complexes with DNA and topoisomerase have a high potential to act as DNA-targeting anticancer drugs [48].

3.7. Molecular docking

3.7.1. Molecular docking of complex **1** with DNA

Molecular docking technique is an attractive scaffold to understand the drug–DNA interactions for the rational drug design and discovery, as well as in the mechanistic study by placing a small molecule into the binding site of the target specific region of the DNA mainly in a non-covalent fashion, although covalent bond may also be formed with reactive ligand and to predict the correct binding mode and binding affinities [49]. Different structural properties lead to different binding modes; in fact one of the most important factors governing the binding mode is the molecular shape. Literature reveals that the forces maintaining the stability of DNA–intercalator complex include van der Waals, hydrogen bonding, hydrophobic charge transfer and electrostatic complementarity [50]. In our experiment, complex **1** was successively docked with DNA duplex of sequence d(CGCGAATTCGCG)$_2$ dodecamer (PDB ID: 1BNA) in order to predict the chosen binding site along with preferred orientation of the ligand inside the DNA minor groove. The energetically most favorable conformation of the docked pose (Fig. 7) revealed that complex **1** strongly binds to minor groove of DNA following the intercalating ligand which prefers the narrower A–T (~10.8 Å) regions compared to G–C (~13.2 Å) ones, and slightly bends the DNA in such a way that a part of the planar phenanthroline rings makes favorable stacking interactions between DNA base pairs and lead to van der Waals interaction with the DNA functional groups which define the stability of groove [51]. On the other hand, electrostatic interactions existing between cationic core of Sn^{IV} metal ion and oxygen atom of the phosphate backbone of DNA double helix. The resulting relative binding energy of docked structure was found to be −307.8 KJ mol^{-1}, indicating the more potent the binding affinity between DNA and complex **1**, correlating well with the experimental DNA binding studies and minor groove binder using DAPI assay. Thus, we can concluded that there is a mutual complement between spectroscopic techniques and molecular docking, which can provide reliable and quick information on the capability of new drugs to interact with DNA.

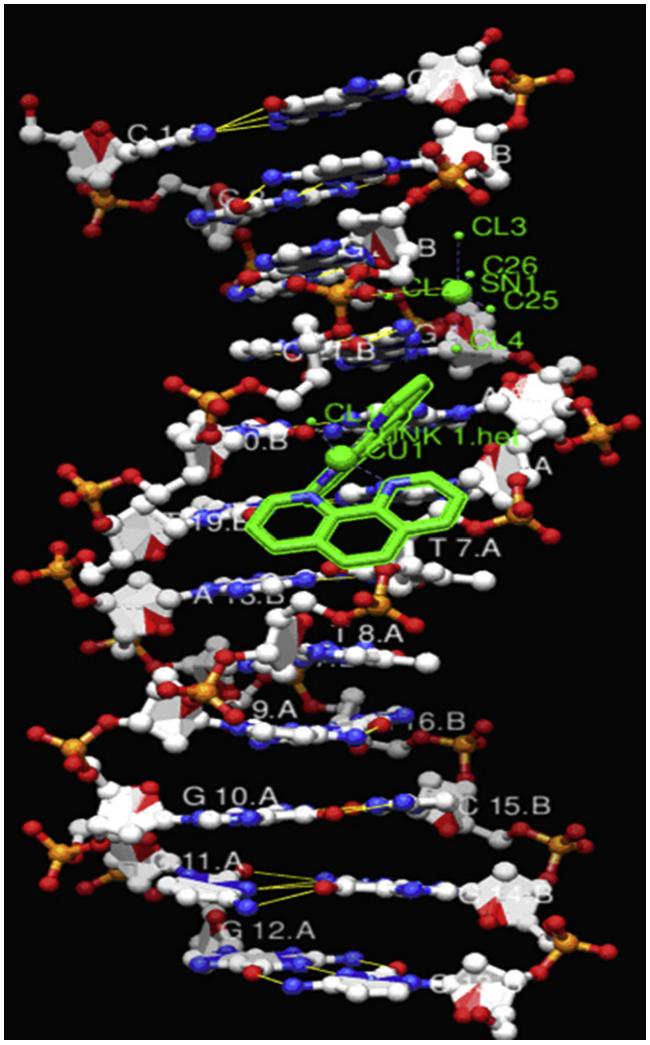

Fig. 7. Molecular docked model of complex **1** showing partial intercalation into adjacent A/T base pairs from minor side with DNA dodecamer duplex of sequence d(CGCGAATTCGCG)$_2$ (PDB ID: 1BNA).

3.7.2. Docking study of complex **1** with DNA-Topo I

In order to determine the observed Topo I inhibitory assay with complex **1**, molecular docking studies were performed to understand the binding mode of complex **1** with human–DNA–Topo I complex (PDB ID: 1SC7) as depicted in Fig. 8(a and b). The X-ray crystallographic structure of human Topo I covalently bound to double-stranded DNA was retrieved from Protein Data Bank and the structure was modified as follows: the phosphoester bond of G12 in

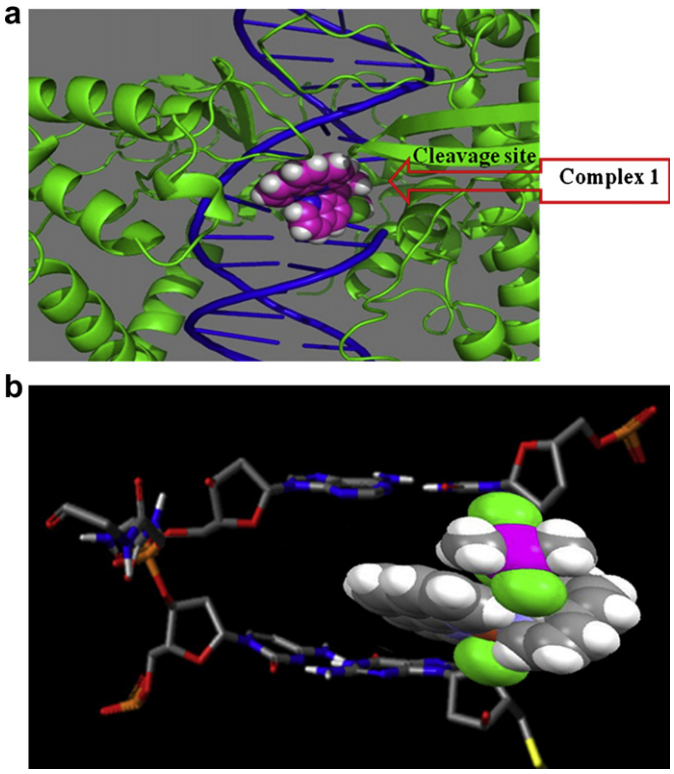

Fig. 8. (a) Molecular docked model showing intercalation of complex **1** in the cleavage site of human DNA Topo I (PDB ID: 1SC7). (b) View is a cut–out of sequence 5′-AAAAAGACTTsX–GAAAATTTTT-3′ showing complex **1** (space filling model) docked in DNA sequence between scissile and non-scissile strand.

1SC7 was rebuilt, and the SH of in which phosphoester bond of G12 in 1SC7 was rebuilt and SH of G11 on the scissile strand was changed to OH [52]. The resulting docking model revealed a dual binding mode of action of the most potent Topo I inhibitor complex **1**, due to its spatial orientation of the interacting phenanthroline rings as well as hydrogen bond accepting moiety. As shown in Fig. 8b, one phenanthroline ring intercalated between the purine ring of G11 (+1) and pyrimidine ring of T10 (−1) in the minor groove on the scissile strand and C112 and A113, on the non-scissile strand, parallel to the plane of base pairs without having hydrogen bonds with the Topo I whereas, another phenanthroline ring facing perpendicularly to the plane of base pairs were functioned as a DNA intercalator which strongly block the rejoining process of the phosphoester. On the other hand, cationic core of second metal ion Sn^{IV} surrounded by chlorine atoms acts as a hydrogen bond acceptor and forms H-bond with Asn 722 residue, which is considered an important amino acids that interact with the ligand in the DNA–top I active site, subsequently leading to inhibitory effect on Topo I [53]. Furthermore, DNA intercalating forces was much more important than hydrogen bonding of the ligand to the surrounding amino acids residues of the protein, or to the base pairs [54]. Our molecular docking study proved the importance of DNA intercalation of complex **1** and the hydrogen bonding. Thus, computer-aided molecular docking studies afford valuable information of drug binding mode in the active site of DNA-Topo I leading to the rational design of new classes of anticancer drugs targeting Topo I.

4. Conclusions

In this work, we have designed and synthesized a novel heterobimetallic complex **1** possessing Cu^{II}–Sn^{IV} metallic cores to act as a potential antitumor agent for use in chemotherapy. The complex **1** was characterized by elemental analysis, IR, UV–vis, molar conductance measurements and X-ray crystallography. The *in vitro* DNA binding studies of complex **1** were carried out to examine its effect on DNA binding propensity and these studies reveal the intercalative mode of binding, in addition to selective binding to the minor groove of DNA in A/T rich sequences. The complex **1** binds supercoiled plasmid pBR322 DNA and displays efficient hydrolytic cleavage as ascertained by gel electrophoretic assays. This could be attributed to its dual binding affinity of metal ions in particular, Sn^{IV} which is generally a specific recognition element for hydrolytic cleavage. The hydrolytic cleavage mechanism of the complex **1** is supported by evidence from DNA relegation employing T4 DNA ligase assay and was validated from free radical quenching. Furthermore, complex **1** exhibits high inhibitory effect on Topo I at a very low concentration ~15 μM. This work therefore, features the design of novel metal-based topoisomerase inhibitors, which are specific DNA groove binders. Such complexes are capable of blocking the essential processes {prevent entanglement of DNA strands during DNA replication, RNA synthesis from DNA (transcription), exchanges of DNA segments between chromosomes (recombination) and elimination of erroneous DNA sequences (repair)}, leading to cell death. Therefore, complex **1** is a potential antitumor drug entity which warrants further *in vitro* and *in vivo* antitumor investigations.

5. Experimental protocols

5.1. General and instrumental

All reagents were commercially available and used as supplied without further purification. Copper chloride dihydrate (Merck), 1,10-phenanthroline, dimethyltin dichloride and Calf thymus DNA (CT DNA), adenosine 5′-monophosphate disodium salt (5′-AMP) (Sigma–Aldrich Chem. Co.), thymidine 5′-monophosphate disodium salt (5′-TMP) were purchased from Fluka, and were stored at 4 °C. 6X loading dye (Fermental Life Science) and Supercoiled plasmid DNA pBR322 (Genei), T4 DNA ligase enzyme and Human-Topo I (CalBioChem), were utilized as received.

Carbon, hydrogen and nitrogen contents were determined on Carlo Erba Analyser Model 1106. Molar conductance was measured at room temperature on Eutech con 510 electronic conductivity bridge. IR spectrum was recorded on Interspec 2020 FTIR spectrometer in KBr pellets from 400 to 4000 cm^{-1}. The ^{1}H and ^{31}P NMR spectra were obtained on a Bruker DRX-400 spectrometer operating at room temperature. Electrospray mass spectra were recorded on Micromass Quattro II triple quadrupol mass spectrometer. FAB mass spectra were recorded on Jeol SX 102/Da-600 mass spectrometer/Data system using Argon/Xenon (6 kv), 10 mA0 as the FAB gas. Electronic spectrum was recorded on UV–1700 PharmaSpec UV–vis spectrophotometer (Shimadzu) in methanol using cuvettes of 1 cm path length. Data were reported in λ_{max}/nm. Fluorescence measurements were determined on a Hitachi F-2500 fluorescence spectrophotometer. The viscosity measurements were carried out using Oswald capillary viscometer maintained at 25 °C.

5.2. Synthesis of heterobimetallic complex, $C_{26}H_{22}Cl_4CuN_4Sn$, **1**

To a stirred methanolic solution (15 ml) of $CuCl_2{\cdot}2H_2O$ (0.170 g, 1 mmol) were simultaneously added drop wise methanolic solution (10 ml) of Me_2SnCl_2 (0.219 g, 1 mmol) and 1,10-phenanthroline monohydrate (0.396 g, 2 mmol) to obtain a clear blue solution. The resulting solution was continuously stirred overnight at room temperature; the resulting homogeneous dark blue reaction mixture was filtered. Blue block crystals suitable for X-ray diffraction were obtained by slow evaporation of the filtrate after a couple of days. Yield: 32%. Anal. Calc. for $C_{26}H_{22}Cl_4CuN_4Sn$: C, 43.77; H, 3.11; N, 7.86%. Found: C, 43.90; H, 3.98; N, 7.99%. Selected IR data (KBr, cm^{-1}) 1651 $\nu(C{-}N)_{phen}$, 842, 706 $\nu(C{-}H)_{phen}$, 594 $\nu(Cu{-}N)$, 331 $\nu(Sn{-}Cl)$. Molar conductance, Λ_M (1×10^{-3} M, DMSO): 74 Ω^{-1} cm^2 mol^{-1} (1:1 electrolyte). UV–vis (10^{-4} M, DMSO, nm, ε): 271 (24024), 295 (8702), 726 (d–d band) 891 (sh).

5.3. X-ray crystallography

Suitable X-ray quality crystals of the copper complex **1** were obtained after slow evaporation of the reaction mixture at room temperature. Single crystal X-ray structural studies of complex was performed on a CCD Oxford Diffraction Xcalibur Saphir 3 diffractometer employing graphite-monochromated Mo-Kα radiation generated from a fine-focus sealed tube ($\lambda = 0.71073$ Å) at 140(2) K. Data collection strategy was evaluated by using the CrysAlisPro CCD software. Collections of data were observed by the standard ω scan techniques and were scaled and reduced using CrysAlisPro RED software. The structure was solved by direct methods using SIR-97 [55] and refined by least-squares methods on F2 using SHELXL-97 [56]. The positions of all atoms were obtained by direct methods. Anisotropic thermal parameter were assigned to all non-hydrogen atoms and the remaining hydrogen atoms were placed in geometrically constrained position and refined as riding atoms with a common fixed isotropic thermal parameter. The drawing of the complex was realized with PLATON [57]. A summary of the selected crystallographic information is given in Table 3.

Table 3
Selected crystallographic data for the complex **1**.

Parameter	
Empirical formula	$C_{26}H_{22}Cl_4CuN_4Sn$
Formula weight (g mol^{-1})	714.51
Crystal system	Monoclinic
Space group	$P2_1/c$
a (Å)	9.5867(2)
b (Å)	12.9048(2)
c (Å)	21.7031(3)
α (deg)	90.00
β (deg)	95.225
γ (deg)	90.00
V (Å^3)	2673.83(8)
Z	4
D_{calc} (Mg m^{-3})	1.775
μ (mm^{-1})	2.153
F (000)	1412
Crystal size (mm)	0.32 × 0.18 × 0.18
Temp (K)	140(2)
Measured reflections	20,390
Unique reflections	5838
θ range (deg)/completeness (%)	2.9–27.00
No. of data/parameters/restraints	5838/326/0
GOF[a]	1.14
$R^b[I > 2\sigma(I)]$	0.041
wR_2[b] (all data)	0.101
Largest diff. peak/hole (e Å^{-3})	0.93/−0.06

[a] GOF is defined as $\{\sum[w(F_0^2 - F_c^2)]/(n-P)\}^{1/2}$ where n is the number of data and p is the number of parameters.
[b] $R = \{\sum||F_0| - |F_c||/\sum|F_0|, wR^2 = \{\sum w(F_0^2 - F_c^2)^2/\sum w(F_0^2)^2\}^{1/2}$.

5.4. DNA binding and cleavage experiments

DNA binding experiments include absorption spectral traces, emission spectroscopy and viscosity conformed to the standard methods and practices previously adopted by our laboratory [58–61]. While measuring the absorption spectra an equal amount of DNA was added to both the compound solution and the reference solution to eliminate the absorbance of the CT DNA itself, and Tris buffer was subtracted through base line correction.

The cleavage experiments of supercoiled pBR322 DNA (300 ng) by complex **1** (5–25 μM) in Tris–HCl/NaCl (5:50 mM) buffer at pH 7.2 was carried out using agarose gel electrophoresis. The samples were incubated for 45 min at 310 K. A loading buffer containing 25% bromophenol blue, 0.25% xylene cyanol, 30% glycerol was added and electrophoresis was carried out at 50 V for 1 h in Tris–HCl buffer using 1% agarose gel containing 1.0 mg/ml ethidium bromide. The DNA cleavage with added reductant was monitored as in case of cleavage experiment without added reductant using agarose gel electrophoresis.

5.4.1. Religation experiment with T4 DNA ligase enzyme

The DNA religation experiments were performed using T4 DNA ligase enzyme to support the hydrolytic mechanism of DNA cleavage by following the standard DNA religation protocol [62]. The complex **1** treated with pBR322 plasmid DNA (2 mg), ligation buffer of 1.5 ml in 10X, T4 DNA ligase 1 ml (2 units) and 2.5 ml of H_2O were mixed and incubated at 4 °C for 1 h. Subsequently, the samples were loaded on 1% agarose gel and visualized by staining with an ethidium bromide solution.

5.5. Topoisomerase I inhibition assay

Human DNA topoisomerase I (Topo I) was purchased from CALBIOCHEM and was used without further purification. One unit of the enzyme was defined as completely relax 1 μg of negatively supercoiled pBR322 DNA in 30 min at 310 K under the standard assay conditions. The reaction mixture (30 μL) contained 35 mM Tris–HCl (pH 8.0), 72 mM KCl, 5 mM $MgCl_2$, 5 mM DTT, 2 mM spermidine, 0.1 mg/ml BSA, 0.25 μg pBR322 DNA, 2 Unit Topo I and complex **1**. These reaction mixtures were incubated at 310 K for 30 min, and the reaction was terminated by addition of 4 μL of 5X buffer solution consisting of 0.25% bromophenol blue, 4.5% SDS and 45% glycerol. The samples were electrophoresed through 1% agarose in TBE at 30 V for 8 h.

5.6. Molecular docking

The rigid molecular docking studies were performed by using HEX 6.1 software [63], is an interactive molecular graphics program for calculating and displaying feasible docking modes of a pairs of protein, enzymes and DNA molecule. The coordinates of metal complex was taken from its crystal structure as a CIF file and was converted to the PDB format using Mercury software (http://www.ccdc.cam.ac.uk/). The crystal structure of the B-DNA dodecamer d(CGCGAATTCGCG)$_2$ (PDB ID: 1BNA) and human–DNA–Topo I complex (PDB ID: 1SC7) were downloaded from the protein data bank (http://www.rcsb.org./pdb). The human–DNA–Topo I complex was prepared using a 5′-bridging phosphorothiolate duplex oligonucleotide [64]. The oligonucleotide sequence of the cleavable strand of the duplex oligomer was 5′-AAAAAGACTTsX–GAAAATTTTT-3′, where 's' represents the 5′-bridging phosphorothiolate of the cleaved strand and 'X' represents any of the four bases A, G, C or T. All calculations were carried out on an Intel pentium4, 2.4 GHz based machine running MS Windows XP SP2 as operating system. Visualization of the docked pose has been done by using CHIMERA (www.cgl.ucsf.edu/chimera) and PyMol (http://pymol.sourceforget.net/) molecular graphics program.

Acknowledgments

The authors (F. Arjmand, S. Parveen and M. Afzal) express their gratitude to Department of Biotechnology, New Delhi, for generous financial support (SchemeNo.BT/PR9205/Med/30/13/2007) and to the Institut de Physique de Rennes, Université de Rennes, Cedex, France, for providing Single Crystal Diffractometer Facility.

Appendix. Supplementary material

Supplementary material associated with this article can be found, in the online version, at doi:10.1016/j.ejmech.2012.01.005.

References

[1] A.M. Pyle, J.K. Barton, Prog. Inorg. Chem. 38 (1990) 413–475.
[2] D.S. Sigman, A. Mazumder, D.M. Perrin, Chem. Rev. 93 (1993) 2295–2316.
[3] T.B. Thederahn, A. Spassky, M.D. Kuwabara, D.S. Sigman, Biochem. Biophys. Res. Commun. 168 (1990) 756–762.
[4] B. Rosenberg, L. VanCamp, J.E. Trosko, V.H. Mansour, Nature (London) 222 (1969) 385–386.
[5] (a) V.G. Vaidyanathan, B.U. Nair, J. Inorg. Biochem. 93 (2003) 271–276; (b) A. Silvestri, G. Barone, G. Ruisi, M.T. Giudice, S. Tumminello, J. Inorg. Biochem. 98 (2004) 589–594.
[6] D.S. Sigman, D.R. Graham, V.D. D' Aurora, A.M. Stern, J. Biol. Chem. 254 (1979) 12269–12272.
[7] T. Ito, S. Thyagarajan, K.D. Karlin, S.E. Rokita, Chem. Commun. (2005) 4812–4814.
[8] Q. Zhang, F. Zhang, W. Wang, X. Wang, J. Inorg. Biochem. 100 (2006) 1344–1352.
[9] F.H. Zelder, A.A. Mokhir, R. Kramer, Inorg. Chem. 42 (2003) 8618–8620.
[10] A.T. Chaviara, P.J. Cox, K.H. Repana, R.M. Papi, K.T. Papazisis, D. Zambouli, A.H. Kortsaris, D.A. Kyriakidis, C.A. Bolos, J. Inorg. Biochem. 98 (2004) 1271–1283.
[11] M. Chauhan, K. Banerjee, F. Arjmand, Inorg. Chem. 46 (2007) 3072–3082.
[12] R.S. Kumar, S. Arunachalam, V.S. Periasamy, C.P. Preethy, A. Riyasdeen, M.A. Akbarsha, Eur. J. Med. Chem. 43 (2008) 2082–2091.
[13] G.N. Kaluderovic, H. Kommera, E. Hey-Hawkins, R. Paschkeb, S. Gómez-Ruiz, Metallomics 2 (2010) 419–428.

[14] M.K. Gounder, A.S. Nazar, A. Saleem, P. Pungaliya, D. Kulkarni, R. Versace, E.H. Rubin, Invest. New Drugs 26 (2008) 205–213.
[15] R. Rao, A.K. Patra, P.R. Chetana, Polyhedron 26 (2007) 5331–5338.
[16] L.-P. Lu, M.-L. Zhu, P. Yang, J. Inorg. Biochem. 95 (2003) 31–36.
[17] G. Valle, S. Calogero, U. Russo, J. Organomet. Chem. 228 (1982) C79–C82.
[18] L.A. Balch, D.E. Oram, Organometallics 7 (1988) 155–158.
[19] S.-W. Ng, C.L. Barnes, D. van der Helm, J.J. Zuckerman, Organometallics 2 (1983) 600–608.
[20] H.F. Yang, C.C. Huang, H.H. Zhang, Y.X. Liu, Z.X. Lian, G.C. Xiao, Acta Crystallogr. E60 (2004) m291–m293.
[21] J.K. Barton, A. Danishefsky, J. Goldberg, J. Am. Chem. Soc. 106 (1984) 2172–2176.
[22] T.M. Kelly, A.B. Tossi, D.J. McConnell, T.C. Strekas, Nucleic Acids Res. 13 (1985) 6017–6034.
[23] F. Schaeffer, S. Rimsky, A. Spassky, J. Mol. Biol. 260 (1996) 523–539.
[24] J.M. Veal, R.L. Rill, Biochemistry 30 (1991) 1132–1140.
[25] D.S. Sigman, Biochemistry 29 (1990) 9097–9105.
[26] (a) N.A. Berger, G.L. Eichhorn, Biochemistry 10 (1971) 1847–1857;
(b) R. Jastrzab, J. Inorg. Biochem. 103 (2009) 766–773.
[27] L.G. Marzilli, Prog. Inorg. Chem. 23 (1977) 255–378.
[28] (a) P. Yang, M. Guo, Met. Based Drugs 5 (1998) 41–58;
(b) F. Arjmand, F. Sayeed, S. Parveen, J. Organomet. Chem. 696 (2011) 3836–3845.
[29] (a) A.H.J. Wang, Curr. Opin. Struct. Biol. 2 (1992) 361–368;
(b) L. Fin, P.J. Yang, J. Inorg. Biochem. 68 (1997) 79–83.
[30] J. Tan, L. Zhu, B. Wang, Dalton Trans. (2009) 4722–4728.
[31] J.B. Lepecq, C. Paoletti, J. Mol. Biol. 27 (1967) 87–106.
[32] O. Stern, M. Volmer, Z. Phys. 20 (1919) 183–188.
[33] K. Midorikawa, S. Kawanishi, FEBS Lett. 495 (2001) 187–190.
[34] A.E. Friedman, C.V. Kumar, N.J. Turro, J.K. Barton, Nucleic Acids Res. 19 (1991) 2595–2602.
[35] F. Liu, K. Wang, G. Bai, Y. Zhang, L. Gao, Inorg. Chem. 43 (2004) 1799–1806.
[36] (a) S. Satyanarayana, J.C. Dabrowiak, J.B. Chaires, Biochemistry 31 (1992) 9319–9324;
(b) L. Kapicak, E.J. Gabbay, J. Am. Chem. Soc. 97 (1975) 403–408.
[37] C. Liu, L. Wang, Dalton Trans. (2009) 227–239.
[38] (a) L.A. Basile, A.L. Raphael, J.K. Barton, J. Am. Chem. Soc. 109 (1987) 7550–7551;
(b) J.N. Burstyn, K.A. Deal, Inorg. Chem. 32 (1993) 3585–3586.
[39] M.E. Branum, A.K. Tipton, S. Zhu, L. Que Jr., J. Am. Chem. Soc. 123 (2001) 1898–1904.
[40] M. Scarpellini, A. Neves, R. Hörner, A.J. Bortoluzzi, B. Szpoganics, C. Zucco, R.A.N. Silva, V. Drago, A.S. Mangrich, W.A. Ortiz, W.A.C. Passos, M.C.B. de Oliveira, H. Terenzi, Inorg. Chem. 42 (2003) 8353–8365.
[41] B. Montaner, W. Castillo-Avila, M. Martinell, R. Ollinger, J. Aymami, E. Giralt, R. Perez-Tomas, Toxicol. Sci. 85 (2005) 870–879.
[42] K. Suzuki, F. Shono, M. Uyeda, Biosci. Biotechnol. Biochem. 62 (1998) 2073–2075.
[43] K. Suzuki, M. Uyeda, Biosci. Biotechnol. Biochem. 66 (2002) 1706–1712.
[44] J.M. Fortune, L. Velea, D.E. Graves, T. Utsugi, Y. Yamada, N. Osheroff, Biochemistry 38 (1999) 15580–15586.
[45] F. Gao, H. Chao, J.Q. Wang, Y.X. Yuan, B. Sun, Y.F. Wei, B. Peng, L.N. Ji, J. Biol. Inorg. Chem. 12 (2007) 1015–1027.
[46] F. Gao, H. Chao, F. Zhou, X. Chen, Y.F. Wei, K.Z. Zheng, L.N. Ji, J. Inorg. Biochem. 102 (2008) 1050–1059.
[47] (a) W. Shi, S.L. Marcus, T.L. Lowary, Bioorg. Med. Chem. 19 (2011) 603–612;
(b) L. Janovec, M. Kozurková, D. Sabolová, J. Ungvarský, H. Paulíková, J. Plsíková, Z. Vantová, J. Imrich, Bioorg. Med. Chem. 19 (2011) 1790–1801.
[48] S. Basili, G. Basso, A. Faccio, A. Granyhan, H. Ihmels, S. Moro, G. Viola, ChemMedChem 3 (2008) 1671–1676.
[49] H. Ihtshamul, J. Ladbury, J. Mol. Recog. 13 (2000) 188–197.
[50] (a) M. Baginski, F. Fogolari, J.M. Briggs, J. Mol. Biol. 274 (1997) 253–267;
(b) E.M. Proudfoot, J.P. Mackay, P. Karuso, Biochemistry 40 (2001) 4867–4878.
[51] R. Filosa, A. Peduto, S. Di Micco, P. de Caprariis, M. Festa, A. Petrella, G. Capranico, G. Bifulco, Bioorg. Med. Chem. 17 (2009) 13–24.
[52] V. Kettmann, D. Kostalova, H.D. Holtje, J. Comput. Aided Mol. Des. 18 (2004) 785–796.
[53] H.T.M. Van, W.-J. Cho, Bioorg. Med. Chem. Lett. 19 (2009) 2551–2554.
[54] X. Xiao, M. Cushman, J. Am. Chem. Soc. 127 (2005) 9960–9961.
[55] A. Altomare, M.C. Burla, M. Camalli, G.L. Cascarano, C. Giocavazzo, A. Guagliardi, A.G.C. Moliterni, G. Polidori, S. Spagna, J. Appl. Crystallogr. 32 (1999) 115–119.
[56] G.M. Sheldrick, SHELX-97 Program for the Refinement of Crystal Structures, University of Göttingen, Germany, 1997.
[57] A.L. Spek, PLATON. A Multipurpose Crystallographic Tool, Utrecht University, Utrecht, The Netherlands, 1998.
[58] M.E. Reicmann, S.A. Rice, C.A. Thomas, P. Doty, J. Am. Chem. Soc. 76 (1954) 3047–3053.
[59] J. Marmur, J. Mol. Biol. 3 (1961) 208–218.
[60] A. Wolfe, G.H. Shimer, T. Meehan, Biochemistry 26 (1987) 6392–6396.
[61] J.R. Lakowiez, G. Webber, Biochemistry 12 (1973) 4161–4170.
[62] X.Q. Chen, X. Peng, J. Wang, Y. Wang, S. Wu, L. Zhang, T. Wu, Y. Wu, Eur. J. Inorg. Chem. 42 (2007) 5400–5407.
[63] D. Mustard, D.W. Ritchie, Proteins: Struct. Funct. Bioinf. 60 (2005) 269–274.
[64] B. Burgin Jr., B.N. Huizenga, H.A. Nash, Nucleic Acids Res. 23 (1995) 2973–2979.